COMMUNICATIONS IN COMPUTATIONAL PHYSICS
Vol. **2**, No. 6, pp. 1184-1198

Commun. Comput. Phys.
December 2007

Dynamics of Defect Motion in Nematic Liquid Crystal Flow: Modeling and Numerical Simulation

Chun Liu[1], Jie Shen[2,*] and Xiaofeng Yang[2]

[1] *Department of Mathematics, Pennsylvania State University, University Park, PA 16802, USA.*
[2] *Department of Mathematics, Purdue University, West Lafayette, IN 47907, USA.*

Received 2 January 2007; Accepted (in revised version) 10 April 2007

Available online 2 August 2007

Abstract. The annihilation of a hedgehog-antihedgehog pair in hydrodynamics of (elastically isotropic) nematic liquid crystal materials is modeled using the Erickson-Leslie theory which results in a nonlinear system for the flow velocity field and liquid crystal director field coupled through the transport of the directional order parameter and the induced elastic stress. An efficient and accurate numerical scheme is presented and implemented for this coupled nonlinear system in an axi-symmetric domain. Numerical simulations of annihilation of a hedgehog-antihedgehog pair with different types of transport are presented. In particular, it is shown that the stretching parameter in the transport equation contributes to the symmetry breaking of the pair's moving speed during the dynamics of annihilation.

AMS subject classifications: 76T99, 76D05, 65N35

Key words: Hedgehog-antihedgehog, liquid crystal, Navier-Stokes, spectral-Galerkin method, defect motion.

1 Introduction

Liquid crystal is often viewed as the fourth state of the matter besides the gas, liquid and solid, or as an intermediate state between liquid and solid. It possesses no or partial positional order, while at the same time, displays an orientational order. To illustrate this special orientational ordering, a (nematic) liquid crystal molecule is often pictured as a rod whose orientation is depicted by the director field $\boldsymbol{d}$. This nematic phase is the simplest of liquid crystal phases and is close to the liquid phase. The molecules float around as in a liquid phase, but have the tendency of aligning along a preferred direction due to their orientation.

*Corresponding author. *Email addresses:* liu@math.psu.edu (C. Liu), shen@math.purdue.edu (J. Shen), xfyang@math.purdue.edu (X. Yang)

In order to capture the coupling between the flow field and the dynamics of the director field, we will start with the following simplified system modeling the motion of nematic phase of liquid crystal flows (cf. [1,2]):

$$\begin{cases} \dfrac{\partial \boldsymbol{u}}{\partial t}+(\boldsymbol{u}\cdot\nabla)\boldsymbol{u}-\mu\nabla\cdot D(\boldsymbol{u})+\nabla p+\lambda\nabla\cdot(\nabla\boldsymbol{d}\otimes\nabla\boldsymbol{d})=0, \\ \nabla\cdot\boldsymbol{u}=0, \\ \dfrac{\partial \boldsymbol{d}}{\partial t}+(\boldsymbol{u}\cdot\nabla)\boldsymbol{d}-\gamma(\Delta\boldsymbol{d}-f(\boldsymbol{d}))=0, \end{cases} \tag{1.1}$$

in a domain $\Omega\in R^3$ filled with liquid crystals, along with initial conditions

$$\boldsymbol{u}(x,0)=u_0; \qquad \boldsymbol{d}(x,0)=\boldsymbol{d}_0, \tag{1.2}$$

and suitable boundary conditions for $\boldsymbol{u}$ and $\boldsymbol{d}$. In the above, $\boldsymbol{u}=(u,v,w)^T$ is the flow velocity and p is the pressure; $\boldsymbol{d}=(d_1,d_2,d_3)^T$ represents the director of the molecules; μ,λ,γ are positive constants representing, respectively, the viscosity of the flow, the coupling coefficient representing the competition parameter between the kinetic energy and the elastic energy, and the parameter of elastic relaxation time; $\nabla\boldsymbol{d}$ is the Jacobian matrix with the (j,k)-th entry to be $\partial\boldsymbol{d}^{(j)}/\partial x_k$, and $\nabla\boldsymbol{d}\otimes\nabla\boldsymbol{d}$ is the Erickson stress tensor whose (j,k)-th entry is $\partial\boldsymbol{d}/\partial x_j\cdot\partial\boldsymbol{d}/\partial x_k$; $D(\boldsymbol{u})=(\nabla\boldsymbol{u}+(\nabla\boldsymbol{u})^T)/2$ is the symmetric part of the strain rate tensor; $\sigma=-pI+2\mu D(\boldsymbol{u})$ is the Newtonian part of the stress tensor. Finally, $f(\boldsymbol{d})=F'(\boldsymbol{d})$ where $F(\boldsymbol{d})$ is the bulk part of the elastic energy. The choice of $F(\boldsymbol{d})$ holds the information on the extensibility of the molecules.

With a set of suitable boundary conditions, the solution $(\boldsymbol{u},\boldsymbol{d})$ of the above system satisfies the following energy identity:

$$\frac{d}{dt}\int_\Omega \frac{1}{2}|\boldsymbol{u}|^2+\frac{\lambda}{2}|\nabla\boldsymbol{d}|^2+\lambda F(\boldsymbol{d})\,dx=\int_\Omega \mu|\nabla\boldsymbol{u}|^2+\lambda\gamma|\Delta\boldsymbol{d}-f(\boldsymbol{d})|^2\,dx. \tag{1.3}$$

The elastic energy in the above system can be viewed as the relaxation as the following Oseen-Franck energy functional for the equilibrium configuration of a unit director field $\boldsymbol{d}$:

$$E(\boldsymbol{d})=\frac{k_1}{2}(\nabla\cdot\boldsymbol{d})^2+\frac{k_2}{2}|\boldsymbol{d}\times(\nabla\times\boldsymbol{d})|^2+\frac{k_3}{2}(\boldsymbol{d}\cdot(\nabla\times\boldsymbol{d}))^2. \tag{1.4}$$

In the elastically isotropic situation, i.e., $k_1=k_2=k_3=k$, this energy can be reduced to the Dirichlet functional $\frac{k}{2}|\nabla\boldsymbol{d}|^2$ plus the null-Lagrangian term which is determined by the boundary anchoring of the director [3]. Furthermore, if we allow the director to stretch at the expense of the bulk energy $F(\boldsymbol{d})$, then we can take $F(\boldsymbol{d})$ to be of the Ginzburg-Landau type, i.e.,

$$F(\boldsymbol{d})=\frac{1}{4\epsilon^2}(|\boldsymbol{d}|^2-1)^2$$

where $\epsilon\ll 1$ is a penalization parameter.

The above simplified system was first proposed by Lin [1,2]. It was motivated by the Erickson-Leslie system describing the flow of nematic liquid crystals. The well-posedness of the system when Ω is bounded was studied in [2]. The method was generalized to the whole Erickson-Leslie system in [4]. The study showed that the simplified system carried most of the mathematical difficulties of the original system, except the kinematic transport of the director field.

In the above system, the transport of the director field due to the flow field is represented by the first two terms of the evolution equation for $\boldsymbol{d}$. It represents the fact that $\boldsymbol{d}(x,t)=\boldsymbol{d}_0(X)$ is purely transported by the flow trajectory $x(X,t)$, where $\boldsymbol{d}_0$ is the initial value of $\boldsymbol{d}$, and

$$x_t(X,t)=\boldsymbol{u}(x,t), x(X,0)=X.$$

Here, X is the initial labeling coordinate of the particle, i.e., the Lagrangian coordinate, while x is the Eulerian coordinate of the particle. Hence the total derivative of the director field is given by

$$\frac{D}{Dt}\boldsymbol{d}=\frac{d}{dt}\boldsymbol{d}(x(X,t),t)=\boldsymbol{d}_t+\boldsymbol{u}\cdot\nabla\boldsymbol{d}.$$

Since $\boldsymbol{d}$ is a vector, we have to take into account its tendency to respond to the stretching in the flow field. Thus, it is natural to look at the deformation tensor F associated with the flow field,

$$F_{ij}=\frac{\partial x_i}{\partial X_j}.$$

A simple application of the chain rule leads to the following transport properties for F [5,6]:

$$\begin{aligned} &F_t+\boldsymbol{u}\cdot\nabla F=\nabla\boldsymbol{u}F,\\ &F_t^{-T}+\boldsymbol{u}\cdot\nabla F^{-T}=-\nabla^T\boldsymbol{u}F^{-T}. \end{aligned} \tag{1.5}$$

Consider first that the liquid crystal molecules are of rod-like shape with infinite aspect ratio. Then, the transport of the direction of the rod, $\boldsymbol{d}$, can be expressed as

$$\boldsymbol{d}(x(X,t),t)=F\boldsymbol{d}_0(X), \tag{1.6}$$

where the stretching of the director besides the transport along the trajectory is clearly taken into account. Taking the derivative with respect to t in the above and using (1.5-1.6), we arrive at

$$\boldsymbol{d}_t+\boldsymbol{u}\cdot\nabla\boldsymbol{d}=F_t\boldsymbol{d}_0+\boldsymbol{u}\cdot\nabla F\boldsymbol{d}_0=\nabla\boldsymbol{u}F\boldsymbol{d}_0=\boldsymbol{d}\cdot\nabla\boldsymbol{u}.$$

Hence the total derivative of the director in this case becomes

$$\frac{D}{Dt}\boldsymbol{d}=\boldsymbol{d}_t+\boldsymbol{u}\cdot\nabla\boldsymbol{d}-\boldsymbol{d}\cdot\nabla\boldsymbol{u}. \tag{1.7}$$

On the other hand, for molecules of ellipsoid shape with finite aspect ratio, the transport in the main axial direction can be represented by

$$\boldsymbol{d}(x(X,t),t)=E\boldsymbol{d}_0(X),$$

where E satisfies the following transport equation:

$$E_t+\boldsymbol{u}\cdot\nabla E=(\alpha\nabla\boldsymbol{u}+(1-\alpha)(-\nabla^T\boldsymbol{u}))F,$$

where α is a positive constant between 0 and 1. In this case, we will have

$$\begin{aligned}\frac{D}{Dt}\boldsymbol{d}&=\boldsymbol{d}_t+\boldsymbol{u}\cdot\nabla\boldsymbol{d}-\alpha\boldsymbol{d}\cdot\nabla\boldsymbol{u}+(1-\alpha)\nabla^T\boldsymbol{u}\boldsymbol{d}\\&=\boldsymbol{d}_t+\boldsymbol{u}\cdot\nabla\boldsymbol{d}-\Sigma\boldsymbol{d}-(2\alpha-1)A\boldsymbol{d}.\end{aligned}\tag{1.8}$$

In the above, A is the symmetric part of the tensor $\nabla\boldsymbol{u}$ and Σ is the skew part. The above description of the transport of the director $\boldsymbol{d}$ is related to the Jeffery orbit of the molecules in the surrounding flow fields, and the Johnson-Segalman transport in viscoelasticity [3,7]. The constant α is associated with the aspect ratio r of the ellipsoid particles (by the formula $2\alpha-1=\frac{r^2-1}{r^2+1}$ or the slippery constant between the flow and the particle. It is clear that when α is near 1, which corresponding to r close to infinity, the rod like particles, then the transport is a purely covariant stretching (parallel transport in the language of differential geometry). When α is close to 0, r is close to 0, the disc like particles, the transport is anti-stretching. And finally, when α is close to $1/2$, then r is close to 1, the particles take the spherical shape and the transport is just the rigid rotation and the transport of the center of the mass. In the literature of liquid crystals, it is also associated with the alignment angle of the molecules in the shear flow situations (however in that case, the constant α will be out of the region $[0,1]$) [3,8].

Taking into account these more general transport of the liquid crystal molecules, the system (1.1) should be modified as follows:

$$\begin{cases}\dfrac{\partial\boldsymbol{u}}{\partial t}+(\boldsymbol{u}\cdot\nabla)\boldsymbol{u}-\mu\nabla\cdot D(\boldsymbol{u})+\nabla p+\lambda\nabla\cdot(\nabla\boldsymbol{d}\otimes\nabla\boldsymbol{d})\\\qquad\qquad-\lambda\nabla\cdot(\beta(\Delta\boldsymbol{d}-f(\boldsymbol{d}))\boldsymbol{d}^T+(1+\beta)\boldsymbol{d}(\Delta\boldsymbol{d}-f(\boldsymbol{d}))^T)=0,\\\nabla\cdot\boldsymbol{u}=0,\\\dfrac{\partial\boldsymbol{d}}{\partial t}+(\boldsymbol{u}\cdot\nabla)\boldsymbol{d}+\beta(\nabla\boldsymbol{u})\boldsymbol{d}+(1+\beta)(\nabla\boldsymbol{u})^T\boldsymbol{d}-\gamma(\Delta\boldsymbol{d}-f(\boldsymbol{d}))=0,\end{cases}\tag{1.9}$$

where we have $\beta=-\alpha$. This model possesses exactly the same energy dissipation law (1.3) as the original system (1.1). However, the different kinematic transport embedded in the system (1.9) will lead to essentially different dynamical phenomena as we will demonstrate with numerical simulations.

More precisely, we study in this paper the annihilation of a hedgehog-antihedgehog pair in both models (1.1) and (1.9). Such phenomena were first carefully observed by Cladis and Brandt in [9]. It is well-known that the point defects are physically different from line defects. In a three-dimensional domain, there is no separation of the scales of the interaction energy between the point defects to the other bulk energy in the regular domain. This is in contrast to the line defects cases, where there is an (logarithmical) infinite concentration of the elastic energy associated with these line defects.The induced

(finite) renormalized energy can then determine the location and the motion of the line defects. The latter phenomena have been both physically verified and mathematically justified rigorously [10]. As to the former case, there are only heuristical/formal argument, using the formal derivation of the interaction energy [3]. However, it is still accepted that the point defects can evolve and annihilate when the orientational configuration is pushed out of equilibrium. Moreover, the relative speed between the two point defect of opposite degree of singularities will be constant, vs the logarithmic acceleration in the two-dimensional (or three-dimensional line defects) cases.

The experiment in [9] was conducted in a cylindrical glass capillary filled with oil. A sufficiently large external perturbation was exerted by varying the temperature. It was observed that when a "thick" capillary was relatively far from the characteristic temperature T_{NA} of the smectic A phase, the hedgehog moved approximately twice as fast as the antihedgehog; while for a "thinner" capillary close to the characteristic temperature T_{NA}, the antihedgehog was almost stationary even with a large initial perturbation. However, such properties are not easy to explain from the theory of harmonic map/heat flow equations [4]. More recently, some numerical simulations on the dynamics of the director, in the absence of the flow field and with anisotropic elastic energy, is reported in [11]. More specifically, they also observed that the hedgehog moves faster than antihedgehog. It should be noted that the effects of elastic forces between the point defects were also studied recently in [12, 13].

In this paper, we study the liquid crystal flow with an isotropic elastic energy. Our main objective is to investigate the effects of the kinematic transport by the flow field on the motion of the point defects. Such transport reflects the geometric nature of the molecules as well as the interaction between the flow field and the liquid crystals. Although the globally averaged flow velocity field is usually small, the local velocity field can still be large due to the presence of the defect singularities, so the effects of transport by the flow field could play a significant role in the dynamics of defect motion.

The paper is organized as follows. In Section 2, we provide the numerical algorithm to simulation the systems. The detailed simulation results will be presented in Section 3. Some concluding remarks are presented in Section 4.

2 Description of the numerical method

We consider a cylinder filled with liquid crystal molecules and assume that the motion and the configuration of the liquid crystals remain to be axial-symmetric so the effective computational domain, in the cylindrical coordinates (r,z), is $D=\{(r,z):0<r<R,0<z<H\}$.

Let $\boldsymbol{u}=(u,v,w)^T$, $\boldsymbol{d}=(d_1,d_2,d_3)^T$, where u, v, w are respectively the velocity components in the axial (r), azimuthal (θ) and vertical (z) directions and d_1, d_2, d_3 are the director fields with respect to (r,θ,z), respectively. In the axial-symmetric cylindrical coordinates,

the gradient and Laplace operators for a scalar function $\phi(r,z)$ are defined by

$$\tilde{\nabla}\phi=(\partial_r\phi,0,\partial_z\phi)^T,\qquad \tilde{\nabla}^2\phi=\partial_r^2\phi+\frac{1}{r}\partial_r\phi+\partial_z^2\phi, \tag{2.1}$$

while the divergence and gradient operators for a vector function $\boldsymbol{u}$ are defined by

$$\tilde{\nabla}\cdot\boldsymbol{u}:=\tilde{\nabla}\cdot(u,v,w)=\frac{1}{r}(ru)_r+w_z, \tag{2.2}$$

and

$$(\tilde{\nabla}\boldsymbol{u})^T=\begin{pmatrix} u_r & v_r & w_r \\ -\dfrac{v}{r} & \dfrac{u}{r} & 0 \\ u_z & v_z & w_z \end{pmatrix}.$$

Thus, the Laplace operator of a vector function $\boldsymbol{u}$ is

$$\tilde{\Delta}\boldsymbol{u}=\tilde{\Delta}(u,v,w)^T=\begin{pmatrix} \tilde{\nabla}^2u-\dfrac{1}{r^2}u & 0 & 0 \\ 0 & \tilde{\nabla}^2v-\dfrac{1}{r^2}v & 0 \\ 0 & 0 & \tilde{\nabla}^2w \end{pmatrix}.$$

Let $[\boldsymbol{f}]_r$, $[\boldsymbol{f}]_\theta$ and $[\boldsymbol{f}]_z$ denote the component of $\boldsymbol{f}$ in the r, θ and z direction. On can verify that:

$$\tilde{\nabla}\cdot(\tilde{\nabla}\boldsymbol{d}\otimes\tilde{\nabla}\boldsymbol{d})=(\tilde{\nabla}\boldsymbol{d})^T\tilde{\Delta}\boldsymbol{d}+\tfrac{1}{2}\tilde{\nabla}(|\tilde{\nabla}\boldsymbol{d}|^2). \tag{2.3}$$

Absorbing the gradient term in the above into the pressure term by defining $\tilde{p}=p+\frac{1}{2}|\tilde{\nabla}\boldsymbol{d}|^2$, we can rewrite the system (1.1) in the axial-symmetric cylindrical coordinates as:

$$\begin{cases} u_t+uu_r-\dfrac{1}{r}v^2+wu_z=-\tilde{p}_r+\mu\left(\tilde{\nabla}^2u-\dfrac{1}{r^2}u\right)-\lambda[(\tilde{\nabla}\boldsymbol{d})^T\tilde{\Delta}\boldsymbol{d}]_r, \\ v_t+uv_r+\dfrac{1}{r}uv+wv_z=\mu\left(\tilde{\nabla}^2v-\dfrac{1}{r^2}v\right)-\lambda[(\tilde{\nabla}\boldsymbol{d})^T\tilde{\Delta}\boldsymbol{d}]_\theta, \\ w_t+uw_r+ww_z=-\tilde{p}_z+\mu\tilde{\nabla}^2w-\lambda[(\tilde{\nabla}\boldsymbol{d})^T\tilde{\Delta}\boldsymbol{d}]_z, \\ \tilde{\nabla}\cdot\boldsymbol{u}=\dfrac{1}{r}(ru)_r+w_z=0, \end{cases} \tag{2.4}$$

and

$$\begin{cases} d_{1t}+ud_{1r}-\dfrac{1}{r}vd_2+wd_{1z}=\gamma\left(\tilde{\nabla}^2d_1-\dfrac{1}{r^2}d_1-[f(\boldsymbol{d})]_r\right), \\ d_{2t}+ud_{2r}+\dfrac{1}{r}vd_1+wd_{2z}=\gamma\left(\tilde{\nabla}^2d_2-\dfrac{1}{r^2}d_2-[f(\boldsymbol{d})]_\theta\right), \\ d_{3t}+ud_{3r}+wd_{3z}=\gamma(\tilde{\nabla}^2d_3-[f(\boldsymbol{d})]_z). \end{cases} \tag{2.5}$$

In order to minimize the effect of the boundary conditions on the defect motion, we choose to use the free-slip boundary condition at both ends of the cylinder, i.e.,

$$\begin{cases} \boldsymbol{u}\cdot\boldsymbol{n}|_{z=0,H}=0, \\ \dfrac{\partial(\boldsymbol{u}\cdot\boldsymbol{\tau})}{\partial\boldsymbol{n}}\Big|_{z=0,H}=0. \end{cases} \tag{2.6}$$

The mathematical analysis for liquid crystal flows with the free-slip boundary condition can be found in [14]. We set the no-slip boundary condition at $r=R$ for the velocity and the homogeneous Neumann boundary condition for the director at both ends of the cylinder and at $r=R$. More precisely,

$$u|_{\Gamma_1\cup\Gamma_3}=0,\quad \partial_{\boldsymbol{n}}u|_{\Gamma_2}=0,\quad v|_{\partial D}=0,\quad w|_{\Gamma_2\cup\Gamma_3}=0, \tag{2.7}$$

$$d_1|_{\Gamma_1}=0,\quad \partial_{\boldsymbol{n}}d_1|_{\partial D\setminus\Gamma_1}=0,\quad d_2|_{\Gamma_1}=0,\quad \partial_{\boldsymbol{n}}d_2|_{\partial D\setminus\Gamma_1}=0,\quad \partial_{\boldsymbol{n}}d_3|_{\partial D\setminus\Gamma_1}=0, \tag{2.8}$$

where $\Gamma_1=\{(r,z):r=0,0<z<H\}$, $\Gamma_2=\{(r,z):0<r<R,z=0 \text{ or } z=H\}$, $\Gamma_3=\{(r,z):r=R,0<z<H\}$.

We now describe our numerical approach. The time discretization is based on a semi-implicit second-order rotational pressure-correction scheme for (2.4) (cf. [15]) and a stabilized semi-implicit scheme for (2.5). To simplify the presentation, we introduce the following notations for the nonlinear terms:

$$\begin{aligned} &\boldsymbol{N}_1(\boldsymbol{u})=-\left(uu_r-\frac{1}{r}v^2+wu_z,uv_r+\frac{1}{r}uv+wv_z,uw_r+ww_z\right)^T, \\ &\boldsymbol{N}_2(\boldsymbol{d})=-\lambda((\tilde{\nabla}\boldsymbol{d})^T\tilde{\Delta}\boldsymbol{d}), \\ &\boldsymbol{N}_3(\boldsymbol{u},\boldsymbol{d})=-(\boldsymbol{u}\cdot\tilde{\nabla})\boldsymbol{d}, \\ &\boldsymbol{N}_4(\boldsymbol{d})=\lambda\nabla\cdot\Big(\beta(\Delta\boldsymbol{d}-f(\boldsymbol{d}))\boldsymbol{d}^T+(1+\beta)\boldsymbol{d}(\Delta\boldsymbol{d}-f(\boldsymbol{d}))^T\Big), \\ &\boldsymbol{N}_5(\boldsymbol{u},\boldsymbol{d})=-\beta(\nabla\boldsymbol{u})\boldsymbol{d}-(1+\beta)(\nabla\boldsymbol{u})\boldsymbol{d}. \end{aligned}$$

Assuming ϕ^k is the numerical solution of ϕ at $t=k\delta t$ when δt is the time step, $(\boldsymbol{u}^k,p^k;\boldsymbol{d}^k)$ and $(\boldsymbol{u}^{k-1},p^{k-1};\boldsymbol{d}^{k-1})$ are known, our time discretization scheme for (2.4) can be described as follows:

- Find an intermediate velocity $\tilde{\boldsymbol{u}}^{k+1}$ such that

$$\begin{cases} \dfrac{3\tilde{\boldsymbol{u}}^{k+1}-4\boldsymbol{u}^k+\boldsymbol{u}^{k-1}}{2\delta t}-\nu\tilde{\Delta}\tilde{\boldsymbol{u}}^{k+1}+\tilde{\nabla}p^k \\ \quad=(2\boldsymbol{N}_1(\boldsymbol{u}^k)-\boldsymbol{N}_1(\boldsymbol{u}^{k-1}))+(2\boldsymbol{N}_2(\boldsymbol{d}^k)-\boldsymbol{N}_2(\boldsymbol{d}^{k-1})), \\ \tilde{u}^{k+1}|_{\Gamma_1\cup\Gamma_3}=0,\quad \partial_{\boldsymbol{n}}\tilde{u}^{k+1}|_{\Gamma_2}=0,\quad \tilde{v}^{k+1}|_{\partial D}=0, \\ \tilde{w}^{k+1}|_{\Gamma_2\cup\Gamma_3}=0. \end{cases} \tag{2.10}$$

- Find an auxiliary function ψ^{k+1} such that

$$\begin{cases} -\tilde{\nabla}^2\psi^{k+1} = \dfrac{3}{2\delta t}\tilde{\nabla}\cdot\tilde{\boldsymbol{u}}^{k+1}, \\ \partial_{\boldsymbol{n}}\psi^{k+1}|_{\partial D} = 0, \end{cases} \tag{2.11}$$

- Update $(p^{k+1},\boldsymbol{u}^{k+1})$ by setting

$$\begin{cases} p^{k+1} = p^k + \psi^{k+1} - \nu\tilde{\nabla}\cdot\tilde{\boldsymbol{u}}^{k+1}, \\ \boldsymbol{u}^{k+1} = \tilde{\boldsymbol{u}}^{k+1} - \dfrac{2\delta t}{3}\tilde{\nabla}\psi^{k+1}. \end{cases} \tag{2.12}$$

- Find $\boldsymbol{d}^{k+1}$ from

$$\begin{cases} \dfrac{3\boldsymbol{d}^{k+1}-4\boldsymbol{d}^k+\boldsymbol{d}^{k-1}}{2\delta t} - \gamma\tilde{\Delta}\boldsymbol{d}^{k+1} = -\gamma(2f(\boldsymbol{d}^k)-f(\boldsymbol{d}^{k-1}) \\ \qquad + \dfrac{s}{\varepsilon^2}(\boldsymbol{d}^{k+1}-2\boldsymbol{d}^k+\boldsymbol{d}^{k-1})) + (2\boldsymbol{N}_3(\boldsymbol{u}^k,\boldsymbol{d}^k)-\boldsymbol{N}_3(\boldsymbol{u}^{k-1},\boldsymbol{d}^{k-1})), \\ d_1^{k+1}|_{\Gamma_1} = 0, \qquad \partial_{\boldsymbol{n}} d_1^{k+1}|_{\partial D\setminus\Gamma_1} = 0, \\ d_2^{k+1}|_{\Gamma_1} = 0, \qquad \partial_{\boldsymbol{n}} d_2^{k+1}|_{\partial D\setminus\Gamma_1} = 0, \quad \partial_{\boldsymbol{n}} d_3^{k+1}|_{\partial D\setminus\Gamma_1} = 0. \end{cases} \tag{2.13}$$

For the modified model (1.9), the only difference is that the equation (2.10) and (2.13) should be modified as follows:

$$\begin{cases} \dfrac{3\tilde{\boldsymbol{u}}^{k+1}-4\boldsymbol{u}^k+\boldsymbol{u}^{k-1}}{2\delta t} - \nu\tilde{\Delta}\tilde{\boldsymbol{u}}^{k+1} + \tilde{\nabla}p^k \\ = (2\boldsymbol{N}_1(\boldsymbol{u}^k)-\boldsymbol{N}_1(\boldsymbol{u}^{k-1})) + (2\boldsymbol{N}_2(\boldsymbol{d}^k)-\boldsymbol{N}_2(\boldsymbol{d}^{k-1})) + (2\boldsymbol{N}_4(\boldsymbol{d}^k)-\boldsymbol{N}_4(\boldsymbol{d}^{k-1})), \end{cases} \tag{2.14}$$

$$\begin{cases} \dfrac{3\boldsymbol{d}^{k+1}-4\boldsymbol{d}^k+\boldsymbol{d}^{k-1}}{2\delta t} - \gamma\tilde{\Delta}\boldsymbol{d}^{k+1} \\ = -\gamma(2f(\boldsymbol{d}^k)-f(\boldsymbol{d}^{k-1}) + \dfrac{s}{\varepsilon^2}(\boldsymbol{d}^{k+1}-2\boldsymbol{d}^k+\boldsymbol{d}^{k-1})) \\ \quad + (2\boldsymbol{N}_3(\boldsymbol{u}^k,\boldsymbol{d}^k)-\boldsymbol{N}_3(\boldsymbol{u}^{k-1},\boldsymbol{d}^{k-1})) + (2\boldsymbol{N}_5(\boldsymbol{u}^k,\boldsymbol{d}^k)-\boldsymbol{N}_5(\boldsymbol{u}^{k-1},\boldsymbol{d}^{k-1})). \end{cases} \tag{2.15}$$

Several remarks are in order:

- We recall that $f(\boldsymbol{d}) = (|\boldsymbol{d}|^2-1)\boldsymbol{d}/\varepsilon^2$, so the explicit treatment of this term usually lead to restrictions on the size of time step δt. We introduced in (2.13) an extra dissipative term $s(\boldsymbol{d}^{k+1}-2\boldsymbol{d}^k+\boldsymbol{d}^{k-1})/\varepsilon^2$, which is of order $s\delta t^2/\varepsilon^2$, to improve the stability while preserving the simplicity. The "shift parameter" s is proportional to the amount of artificial dissipation added in the numerical scheme. Larger s will lead to a more stable but less accurate scheme. Numerical experiments indicate that $s=2$ in the Cartesian coordinates and $s=5$ in the cylindrical coordinates provide a good balance between stability and accuracy.
- At each time step, one only needs to solve a sequence of Poisson-type equations. This is to be accomplished by using the Legendre-Galerkin method (cf. [16–18]).

3 Numerical simulation

In this section, we describe our numerical simulations using the numerical method described in the previous section for the time variable and the Legendre-Galerkin Method (cf. [16, 18, 19]) for the space variable. We consider a cylinder of radius $R=1$ and height $H=4$ filled with liquid crystals. The initial velocity $\boldsymbol{u}^0(r,z)$ is set to be $\mathbf{0}$ and the initial phase of the director field $\boldsymbol{d}^0(r,z)=(d_1^0(r,z),d_2^0(r,z),d_3^0(r,z))$ is set to be

$$d_1^0(r,z)=\tilde{d}_1(r,z)/\sqrt{\tilde{d}_1^2+\tilde{d}_3^2+\varepsilon^2}, \qquad d_2^0(r,z)=0,$$
$$d_3^0(r,z)=\tilde{d}_3(r,z)/\sqrt{\tilde{d}_1^2+\tilde{d}_3^2+\varepsilon^2},$$

where

$$\begin{cases} \tilde{d}_1(r,z)=-\dfrac{1}{1+e^{10(2z/H-1)}}\dfrac{2r}{R}-\left(1-\dfrac{1}{e^{10(2z/H-1)}}\right)\dfrac{2r}{R}, \\ \tilde{d}_3(r,z)=-\dfrac{1}{1+e^{10(2z/H-1)}}(2z/H-2c_1/H)+\left(1-\dfrac{1}{1+e^{10(2z/H-1)}}\right)(2z/H-2c_2/H), \end{cases}$$

where c_1 and c_2 are the initial positions (in the z directions) of the hedgehog and anti-hedgehog.

In all numerical experiments below, we set $c_1=1.5$ and $c_2=2.5$ so that initially the hedgehog and antihedgehog are placed at $(r,z)=(0,1.5)$ and $(0,2.5)$ respectively. We also set $\varepsilon=0.02$, $\nu=1$, $\gamma=1$, $s=5$. The number of grid points in the r direction ranges from $M=128$ to $M=188$, while that in the z directions ranges from $N=256$ to $N=332$; the time step δt ranges from 10^{-3} to 10^{-6}. The values of λ and β are specified in the figure captions.

The initial director field is shown in Fig. 1(a), and the initial contours of $|d|^2$ is shown in Fig. 1(b) where the two singularities are at the lowest energy points.

We are interested in the dynamics of the motion of the hedgehog-antihedgehog pair governed by the system (1.1), and in the effects of coupling coefficient λ and shape parameter β on the annihilation speed of the defects.

(a) We start with the no-flow case, i.e., $\boldsymbol{u}(x,t)=0$ or $\lambda=0$, In Fig. 2 is shown the snapshots of the contours of $|d|^2$ at different times. Fig. 3(a) shows the trajectory of the two defect locations in time. We observe first that the speeds of two defects are exactly the same. Furthermore, we observe from the dotted straight lines in Fig. 3(a) (see also the speeds of the two defects in Fig. 3(b) in th time interval (2,6)) that after an initial transient time and before the final stage where the annihilation speed is significantly accelerated, the speeds of the two defects are essentially constant. This phenomenon is consistent with the heuristical argument in [3] that the relative annihilation speed in three-dimensional cases should be essentially constant.

(b) Next, we take a small coupling coefficient $\lambda=0.01$ and examine the effect of the shape parameter β on the annihilation speed. It is observed that, for this small coupling coeffi-

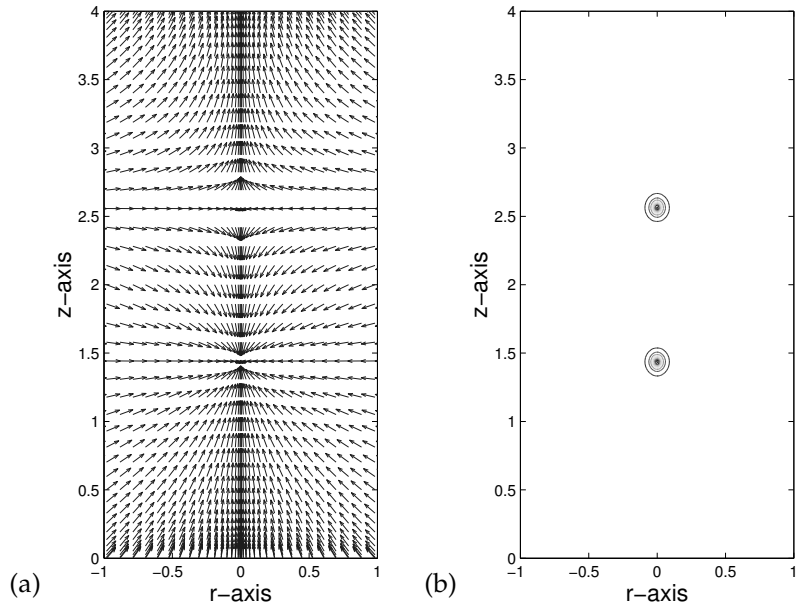

Figure 1: (a) Initial director field (b) Initial contours of $|d|^2$.

cient $\lambda=0.01$, the speeds of the two defects are the same for all β considered, as in the no flow case.

(c) For the last set of numerical experiments, we take a larger coupling coefficient $\lambda=0.03$ and probe the effect of shape parameter β on the annihilation speed.

- We start with $\beta=-0.1$ which represents disc like molecules and decrease gradually to $\beta=-0.5$ which represents spherical shaped molecules. The defect locations for two representative values $\beta=-0.1$ and $\beta=-0.5$ are shown in Fig. 4. We observed that for this range of β, the speeds of the two defects are always the same, while the speed decreases as β decreases.
- We gradually decrease β from -0.5 (spherical shaped molecules) to -0.9 (rod like molecules) and observe that as soon as $\beta<-0.5$ (i.e., the shapes of the molecules become elongated in the axial direction), the speed of the hedgehog becomes faster than that of the antihedgehog, and that as β decreases, the ratio of the hedgehog speed vs. the antihedgehog speed increases. In Fig. 5, we plot the speed ratio of the hedgehog vs. the antihedgehog for $\beta\in[-0.9,-0.1]$ at half of the annihilation time. These results indicate that the combined effects of the flow field (through the coupling coefficient λ) and the shape parameter β can significantly impact the defect dynamics.
- We now provide more details for the case $\beta=-0.9$ which represents rod like molecules. Plotted in Fig. 6 are the snapshots of contours of $|d|^2$ and in Fig. 7(a) are the locations of the two defects. In Fig. 7(b), we plot the speeds of the hedgehog

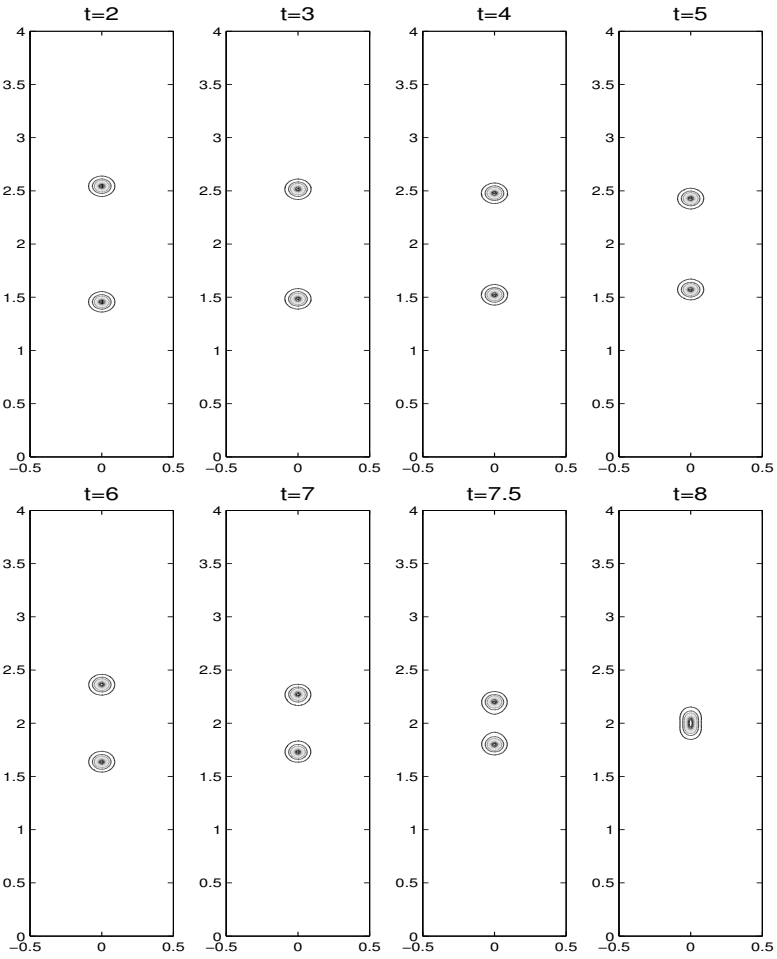

Figure 2: Snapshots of the contours of $|d|^2$ in the no-flow case, i.e., $\lambda=0$.

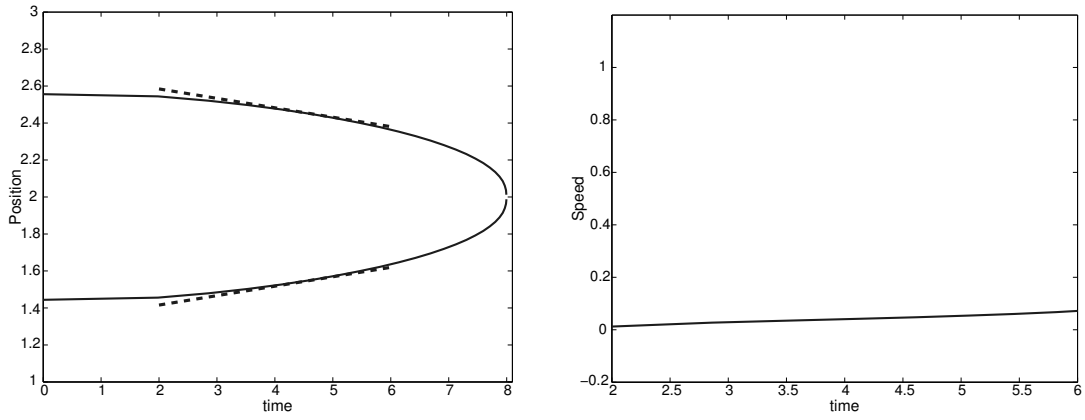

(a) (b)

Figure 3: No-flow case: (a) locations of the two defects, (b) annihilation speed of the two defects.

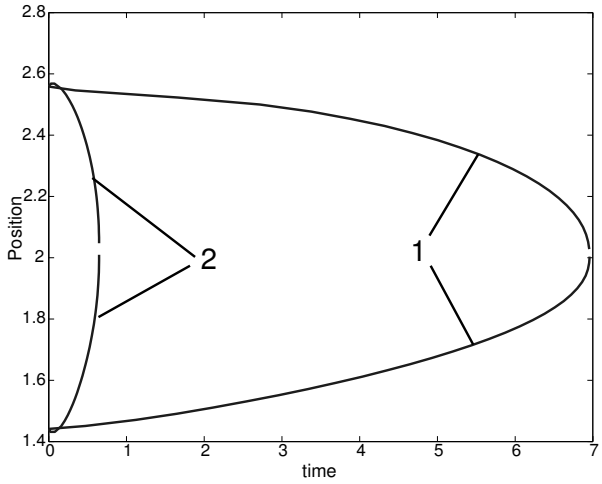

Figure 4: Locations of the hedgehog-antihedgehog defects with $\lambda=0.03$, and (Case 1) $\beta=-0.5$ and (Case 2) $\beta=-0.1$.

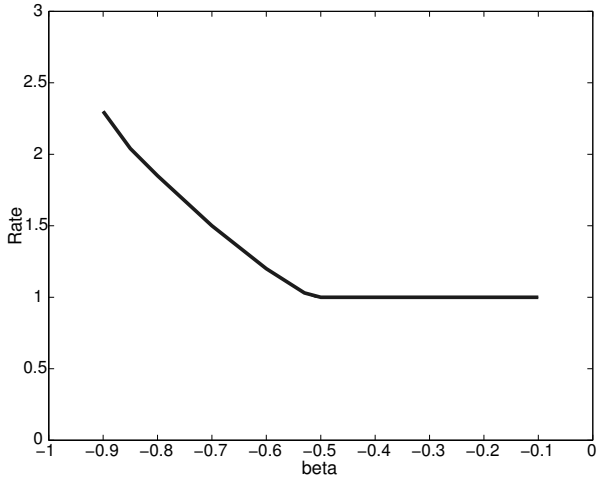

Figure 5: The ratio of the speed of the hedgehog vs. the antihedgehog at the half time of the annihilation, vs. different β values.

and antihedgehog in the time interval (2, 5.5) which excludes the initial transient time interval and the fast moving interval before annihilation. We observe that the moving speed of hedgehog is roughly twice as fast as that of the antihedgehog in the time interval (2, 5.5). We recall that it was reported in [9] that the hedgehog moved twice as fast as the antihedgehog in an elastically anisotropic liquid crystals without flow. In order to show the robustness of this observation with respect to perturbations of β, we plot in Fig. 8 the defect locations with three different values $\beta=-0.85,-0.9,-0,95$.

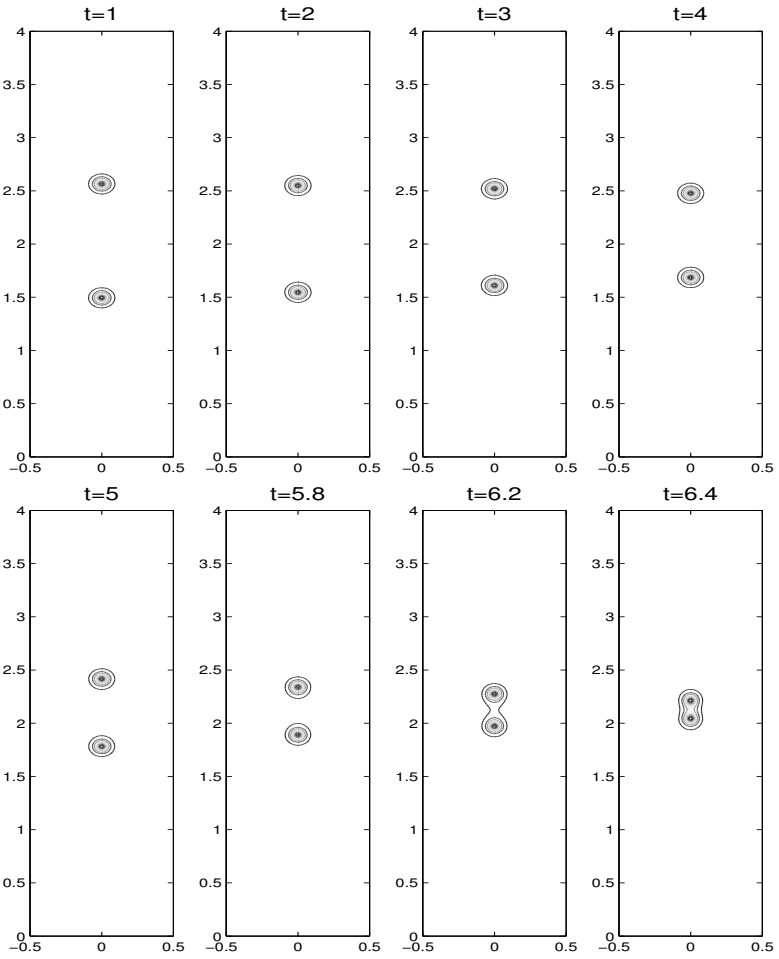

Figure 6: Snapshots of the energy contours with $\beta=-0.9$, $\lambda=0.03$.

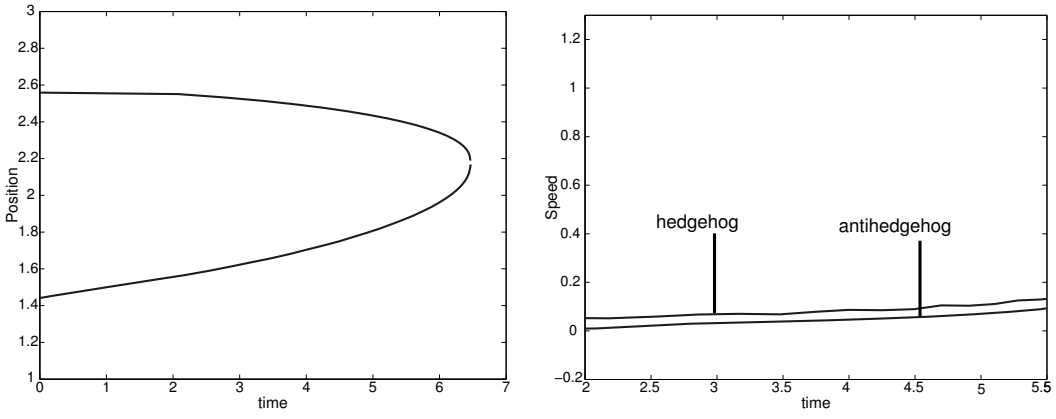

(a) (b)

Figure 7: $\beta=-0.9$, $\lambda=0.03$: (a) locations of the two defects, (b) moving speeds of the two defects.

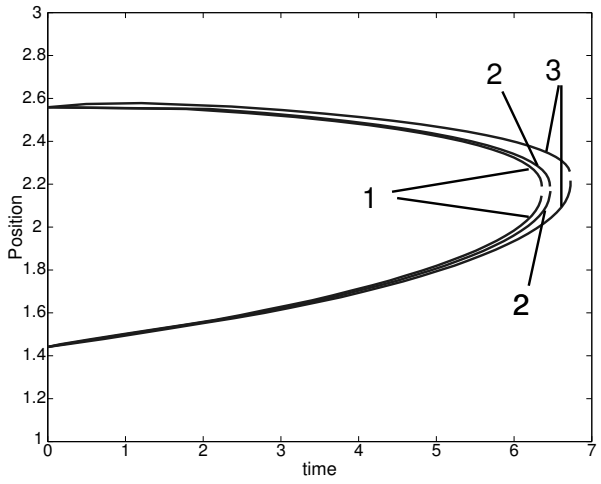

Figure 8: Locations of the two defects for various values of β with $\lambda=0.03$: Case 1: $\beta=-0.85$, Case 2: $\beta=-0.9$, Case 3: $\beta=-0.95$.

4 Concluding remarks

We presented an energetic variational method for modeling and simulating the dynamics of point defects in liquid crystal flows. The stabilized semi-implicit second-order time-marching scheme coupled with the Legendre-Galerkin approximation in space has proved to be efficient and accurate for this class of problems. We presented ample numerical experiments to demonstrate the effects of coupling coefficient λ and the parameter β (which is related to the molecule shape) on the dynamics of annihilation of a hedgehog-antihedgehog pair. Our numerical experiments indicate that despite the fact that the globally averaged flow velocity field is usually small, the flow field can dramatically affect the defect dynamics, since the local field can still be large due to the presence of the defect singularities.

More precisely, our numerical results reveal that for a smaller coupling coefficient (i.e., negligible flow effect), the trajectories of the hedgehog and antihedgehog defects are symmetric while for a larger coupling coefficient (i.e., significant flow effect), this symmetry is broken. Note that this symmetry breaking was observed in [11] for liquid crystals with anisotropic elastic energy in the absence of flow field. Our numerical simulation indicates that this symmetry breaking will also occur with an isotropic elastic energy when the flow is part of the system.

It is observed that the parameter β (which is related to the molecule shape) has a significant impact on the relative moving speed of the two defects: for β in the range of $[-0.5,-0.1]$, the moving speed of the two defects remained to be essentially the same; for β in the range of $[-0.9,-0.5)$ (i.e., the shapes of the molecules are elongated in the axial direction), the moving speed of the hedgehog became faster than that of the antihedgehog, and as β decreases, the speed ratio of the hedgehog vs. the antihedgehog increases.

Acknowledgments

The research of J. Shen and X. Yang is supported in part by NSF grants DMS-0456286, DMS-0509665 and a Purdue Research Foundation PRF-CIRG Grant. The research of C. Liu is supported in part by NSF grant DMS-0405850.

References

[1] F. H. Lin, Mathematics theory of liquid crystals, in: Applied Mathematics at the Turn of the Century, Lecture Notes of the 1993 Summer School, Universidat Complutense de Madrid, 1995.
[2] F. H. Lin and C. Liu, Nonparabolic dissipative systems modeling the flow of liquid crystals, Commun. Pur. Appl. Math., 48 (1995), 501-537.
[3] P. G. de Gennes and J. Prost, The Physics of Liquid Crystals, Oxford University Press, 1993.
[4] F. H. Lin and C. Liu, Static and dynamic theories of liquid crystals, J. Part. Diff. Eq., 14(4) (2001), 289-330.
[5] C. Liu and N. J. Walkington, An Eulerian description of fluids containing visco-elastic particles, Arch. Ration. Mech. Anal., 159(3) (2001), 229-252.
[6] F. H. Lin, C. Liu and P. Zhang, On viscoelastic fluids, Commun. Pur. Appl. Math., 58 (2005), 1-35.
[7] G. B. Jeffery, The motion of ellipsoidal particles immersed in a viscous fluid, Proc. R. Soc. London Ser. A, 102 (1922), 161-179.
[8] N. Kuzzu and M. Doi, Constitutive equation for nematic liquid crystals under weak velocity gradient derived from a molecular kinetic equation, J. Phys. Soc. Jpn., 52 (1983), 3486-3494.
[9] P. E. Clais and H. R. Brand, Hedgehog-antihedgehog pair annihilation to a static soliton, Physica A, 326 (2003), 322-332.
[10] F. H. Lin, Some dynamic properties of Ginzburg-Landau vorticies, Commun. Pur. Appl. Math., 49(4) (1996), 323-359.
[11] M. Svetec, S. Kralj, Z.Bradač and S. Žumer, Annihilation of nematic point defects: Precollision and post-collision evolution, Eur. Phys. J. E, 20 (2006), 71-79.
[12] E. C. Gartland Jr., A. M. Sonnet and E. G. Virga, Elastic forces on nematic point defects, Continuum Mech. Thermodyn., 14(3) (2002), 307-319.
[13] P. Cermelli and E. Fried, The evolution equation for a disclination in a nematic liquid crystal, Proc. R. Soc. London Ser. A, 458(2017) (2002), 1-20.
[14] C. Liu and J. Shen, On liquid crystal flows with free-slip boundary conditions, Discrete Cont. Dyn. Syst., 71 (2001), 307-318.
[15] J. L. Guermond and J. Shen, On the error estimates of rotational pressure-correction projection methods, Math. Comput., 73 (2004), 1719-1737.
[16] J. Shen, Efficient spectral-Galerkin method I. Direct solvers of second and fourth-order equations using Legendre polynomials, SIAM. J. Sci. Comput., 15 (1994), 1489-1505.
[17] J. Shen, Efficient spectral-Galerkin method III. Polar and cylindrical geometries, SIAM. J. Sci. Comput., 18 (1997), 1583-1604.
[18] J. M. Lopez and J. Shen, An efficient spectral-projection method for the Navier-Stokes equations in cylindrical geometries I. Axisymmetric cases, J. Comput. Phys., 139 (1998), 308-326.
[19] F. Marques, J. M. Lopez and J. Shen, Mode interactions in an enclosed swirling flow: A double Hopf between azimuthal wavenumbers 0 and 2, J. Fluid Mech., 455 (2002), 263-281.